BMC Medical Imaging

RESEARCH

Open Access

Comparison of the effects of IMRT and IMPT on MRI features of normal brain tissue: a retrospective study

Jian Xu[1,2], Lili Zhang[3], Tingting Liu[4], Qingzeng Liu[1,2] and Jian Zhu[1,2*]

Abstract

Objective This study aims to analyze magnetic resonance imaging (MRI) feature changes across different dose regions to investigate the differences in imaging feature alterations induced by Intensity-Modulated Radiation Therapy (IMRT) and Intensity-Modulated Proton Therapy (IMPT) in normal brain tissue. And evaluate the potential application value of radiomic features in dose optimization and biological dose assessment.

Methods A retrospective analysis included 113 patients undergoing brain-target radiotherapy: 44 receiving IMPT (average total dose: 5713.63 ± 774.32 cGy) and 69 receiving IMRT (average total dose: 5489.86 ± 627.05 cGy). There was no significant difference in prescribed doses between groups ($p < 0.05$). MRI data were collected pre-treatment and one month post-treatment, including T1, enhanced T1, T2, T2-FLAIR, and ADC sequences. Images underwent preprocessing and rigid registration on the 3D Slicer platform. Dose regions (90%, 70%, 50%, 30% of the total dose) were segmented and classified into high (70–90%), medium (50–70%), and low (30–50%) dose regions as volumes of interest (VOI). Radiomic features were extracted from pre- and post-treatment MRI datasets, and Delta features were calculated as the difference between pre- and post-treatment data. Non-parametric tests, t-tests, and Mann-Whitney U tests were used to identify significant feature changes, with effect size analysis to compare the magnitude of changes. Multiple testing correction was applied to reduce false positives. Finally, box plots and the Mapping of Dose Distribution and Differences in Radiomics Feature Variation were utilized to visually illustrate the extent of brain tissue changes in each dose region following radiotherapy.

Results Non-parametric tests indicated that more radiomic features exhibited significant changes in the IMRT group ($p < 0.001$). Effect size analysis also showed that the majority of features demonstrated greater and more pronounced changes within dose regions in the IMRT group ($p < 0.05$). Further correlation analysis revealed that most features (33/34) had weak correlations with dose-volume parameters ($r < 0.3$), suggesting that treatment modality itself may be the primary driver of these alterations rather than dose distribution alone. This finding highlights the need to refine traditional dose-based radiotherapy evaluation by incorporating biological effect considerations. Additionally, Moreover, the feature Delta_wavelet-HHL.65 exhibited the most significant change, with an effect size of -0.8 in the IMRT group. It demonstrated a moderate-to-high correlation with dose-volume parameters in the medium-to-high dose regions, with a maximum correlation coefficient of 0.65 ($p < 0.001$). This suggests that Delta_wavelet-HHL.65 may

*Correspondence:
Jian Zhu
zhujian@sdfmu.edu.cn

Full list of author information is available at the end of the article

serve as a potential biomarker for reflecting local dose effects, contributing to the optimization of radiotherapy dose distribution.

Conclusions This study revealed that IMRT and IMPT induce distinct radiomic feature changes under comparable dose conditions, and these differences are not solely determined by dose distribution. This suggests that radiotherapy evaluation should extend beyond physical dose metrics to incorporate biological effect dimensions. Furthermore, Delta_wavelet-HHL.65 demonstrated the most pronounced change in the IMRT group and exhibited correlations with dose-volume parameters in the low-to-medium dose regions, highlighting its potential for radiotherapy optimization.

Clinical trial number Not applicable.

Keywords Magnetic resonance imaging, Delta features, Proton radiotherapy, Radiation-related brain injury

Background

Radiotherapy (RT) is an essential modality for cancer treatment. Intensity-Modulated Radiation Therapy (IMRT) and Intensity-Modulated Proton Therapy (IMPT) are two primary radiation therapy techniques, each characterized by distinct dose distribution properties. IMRT utilizes X-rays, which offer excellent dose modulation capabilities. However, as X-rays pass through tissues, their energy gradually attenuates, resulting in higher low-dose radiation exposure to surrounding normal tissues. In contrast, IMPT employs proton beams, whose physical properties allow them to maintain a stable energy level upon entering the tissue until reaching the Bragg peak [1]. In simple terms, protons maintain a low energy level at the entrance to protect proximal normal tissues. As they traverse the tissue and their velocity decreases, their energy is rapidly released at a threshold point and terminates abruptly. If the protons reach the tumor site at this moment, the dose can be precisely concentrated in the tumor region [2], thereby reducing radiation exposure to surrounding tissues [3]. Figure 1 illustrates the differences in dose distribution between protons and photons in two cases of sellar tumors. It demonstrates the dose distribution differences between IMPT (Figure A) and IMRT (Figure B) in treating sellar lesions. Notably, the low-dose radiation from photons (green and blue regions) is more widespread, covering a larger volume of normal brain tissue. In contrast, the high-dose area of protons (red and orange) is more concentrated within the target, with a significantly reduced distribution of low-dose regions, highlighting the advantage of IMPT in minimizing radiation exposure to normal tissues.

However, radiation inevitably affects surrounding normal tissues, and for patients with brain tumors, the potential damage of radiotherapy to normal brain tissue has raised widespread concern. Studies have shown that radiation-induced brain injury may lead to long-term cognitive decline as well as structural and functional damage to brain tissue. Grosshans et al. reported that radiation-induced brain injury exhibits patterns similar to those observed in patients with Alzheimer's disease and stroke, characterized by tau protein abnormalities and synaptic damage. Among the study participants, more than 40% exhibited cognitive decline, particularly in memory and executive functions, within three months after radiotherapy. The negative effects of radiotherapy intensified with increasing treatment doses, leading to significant structural changes in both gray and white matter [4]. Patel et al. conducted a detailed analysis of cognitive decline induced by radiotherapy, highlighting that brain irradiation causes dendritic structural damage, thereby impairing neuronal communication efficiency. Their data indicated that approximately 60% of patients who received doses exceeding 30 Gy experienced symptoms such as memory loss and attention deficits within six months. The study also emphasized the necessity of developing novel protective therapies, such as anti-inflammatory drugs, to mitigate the neurotoxic effects of radiotherapy [5]. Therefore, evaluating and comparing the effects of different radiotherapy modalities on the microstructure and function of normal brain tissue holds significant clinical importance.

Conventional MRI imaging has been widely used to detect brain tissue damage following radiotherapy; however, its ability to assess microstructural alterations remains limited. Radiomics, by extracting a vast array of imaging features, can reveal subtle changes in the tissue microenvironment that are often undetectable by traditional imaging techniques. By analyzing variations in radiomic features across different dose regions, radiomics can help elucidate the mechanisms underlying radiation-induced microstructural damage in normal brain tissue.

Previous studies have demonstrated that MRI-based radiomic features can be used to predict radiation-induced brain injury. Zhang et al. developed a machine learning-based MRI radiomics model for the early detection of radiation-induced brain injury in nasopharyngeal carcinoma patients. Their study analyzed MRI images from 242 patients and constructed three predictive models, achieving areas under the curve (AUCs) of 0.830, 0.773, and 0.716, respectively. These models were capable of predicting radiation-induced temporal lobe injury (RTLI) before its clinical manifestation, thereby

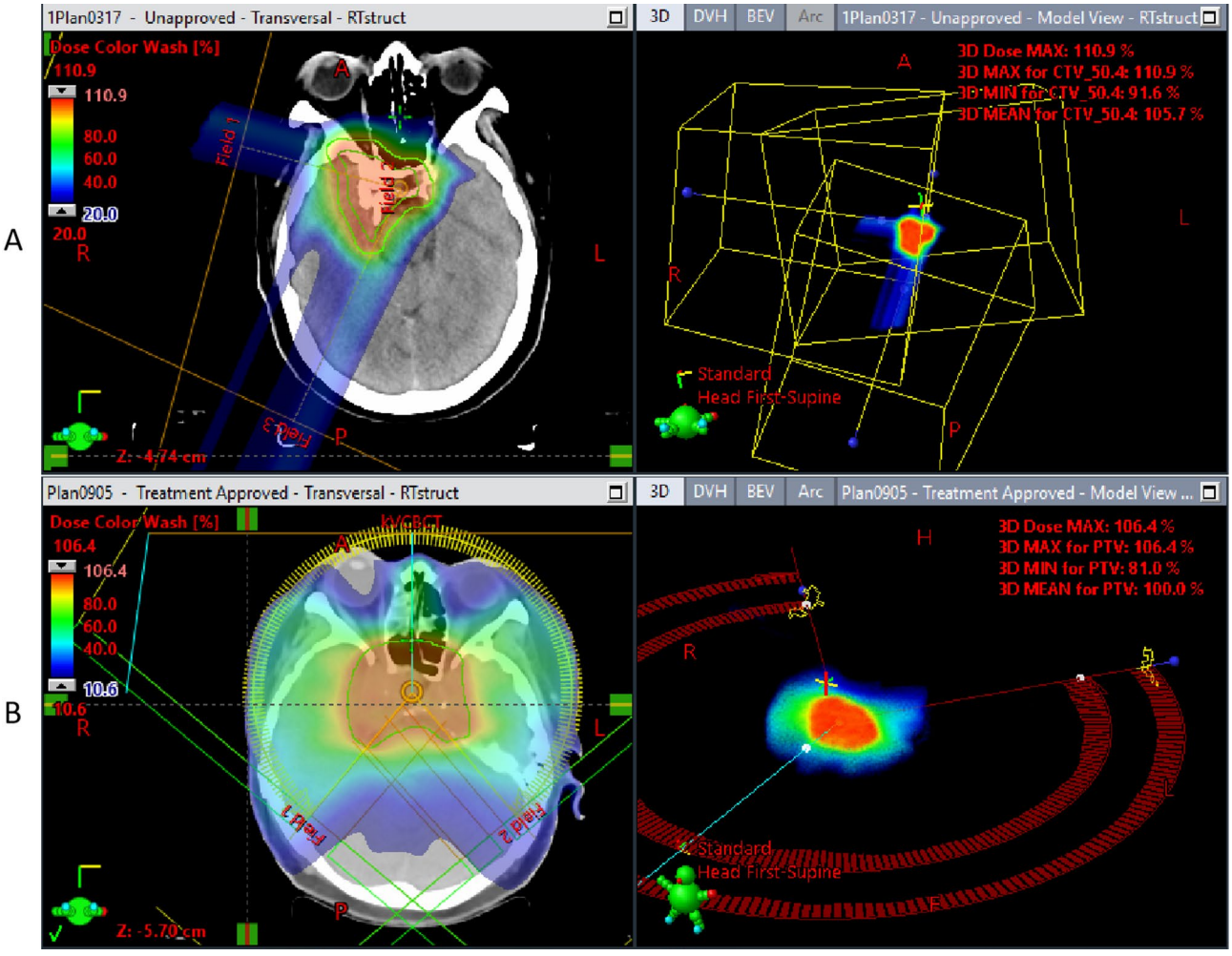

Fig. 1 Dose distribution comparison between photon and proton therapy in patients with sellar region tumors

providing an opportunity for early medical intervention to mitigate the adverse effects of radiotherapy on brain tissue [6]. Similarly, Bao et al. developed a radiomics model based on pre-treatment MRI to predict the risk of RTLI in nasopharyngeal carcinoma patients. Their retrospective analysis included data from 216 patients, and the constructed radiomics model achieved AUCs of 0.89 and 0.92 in the training and validation sets, respectively, significantly outperforming clinical models (AUC = 0.93 and 0.95). Integrating radiomic and clinical features further enhanced predictive accuracy, highlighting the superior performance of radiomics in assessing the risk of radiotherapy-related brain injury [7]. Hou et al. incorporated MRI-based radiomic features with clinical factors to develop a radiomics nomogram model for predicting RTLI. Their study included 203 nasopharyngeal carcinoma patients, and the radiomics model based on T2-weighted imaging (T2WI) integrated 14 key features. The AUCs in the training and validation cohorts were 0.87 and 0.82, respectively, demonstrating significantly improved predictive accuracy compared to models based on either radiomic or clinical features alone. This study underscores that a radiomics nomogram integrating dosimetric and radiomic features can effectively assess RTLI risk, offering strong clinical applicability [8].

Although IMPT provides superior protection for normal tissues compared to IMRT from a dose distribution perspective (as illustrated in Fig. 1), research on the microstructural changes induced by IMRT and IMPT within the same or similar dose regions remains insufficient. By analyzing MRI radiomic feature variations across different dose regions, we aim to preliminarily assess the differential effects of IMRT and IMPT on normal brain tissue at a microstructural level. Additionally, we seek to explore the potential application of radiomic features in dose optimization and biological dose assessment.

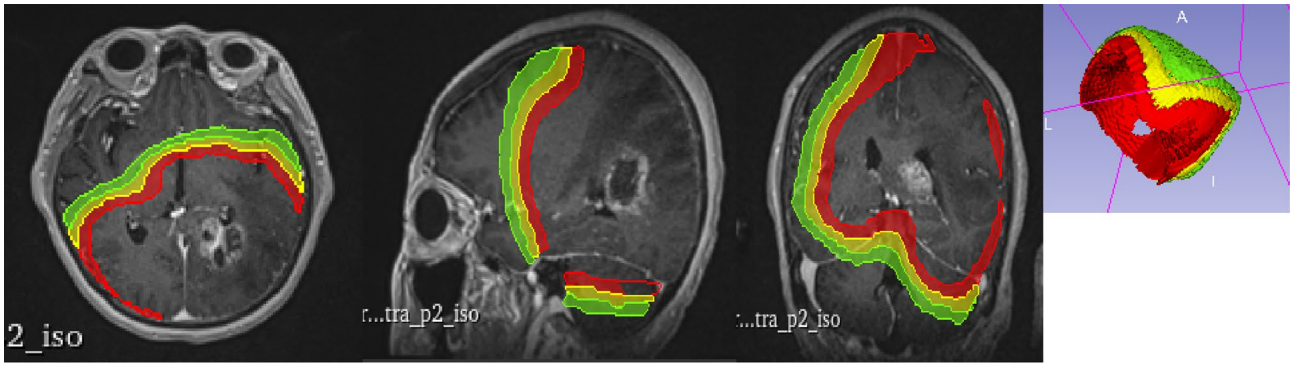

Fig. 2 Segmentation of dose regions on contrast-enhanced T1 images, showing different positions and 3D perspectives

Methods

Data Preparation

This retrospective study included 113 patients (44 IMPT and 69 IMRT) with cranial tumors who underwent radiotherapy at Shandong Cancer Hospital from June 2021 to May 2024. Multi-parametric MRI data, including T1, contrast-enhanced T1, T2, T2-FLAIR, and ADC sequences, were collected for each patient before treatment and one month after treatment.

Preprocessing

Bias field correction was applied using SimpleITK to eliminate signal intensity variations caused by magnetic field inhomogeneity. Images were then resampled to a voxel size of $1 \times 1 \times 1$ mm using B-spline interpolation in `scipy.signal` to minimize the effects of slice thickness variation and isotropic voxels. After outlier pixel removal, all image volumes were scaled within a gray intensity range of 0-255 to reduce inherent pixel intensity differences across various MRI scanners [9].

Segmentation

Using the Varian Eclipse radiotherapy planning system, cumulative dose maps were generated by summing up the fractionated treatment plans for each patient. Preprocessed, pre-treatment contrast-enhanced T1 images were uploaded and registered with planning images, and the "Boolean operations" function of the Eclipse system was used to assist in segmentation. The intersection of dose regions at 90%, 70%, 50%, and 30% of the total prescription dose with the brain parenchyma was extracted and further segmented to create high (70–90%), medium (50–70%), and low (30–50%) dose regions as volumes of interest (VOI).

Registration

The segmented images were uploaded to the 3DSlicer platform (version 5.2.1), where the pre-treatment contrast-enhanced T1 image was used as the fixed image. Rigid registration was performed for the pre- and post-treatment images of other sequences as the moving images.

Table 1 Overview of radiomics features

Feature Type	Examples	Quantity
Shape Features	Major Axis Length, Minor Axis Length, Mesh Area, etc.	14
First-Order Statistical Features	Energy, Kurtosis, Mean, Median, etc.	18
Higher-Order Statistical Features	Autocorrelation, Contrast, Correlation, etc.	75
Wavelet Features	Wavelet Features	744
Total		851

Feature extraction and data integration

Radiomic features for each dose region on each sequence, both pre- and post-treatment, were extracted using the Radiomics module in 3DSlicer, as illustrated in Fig. 2. This produced pre-treatment and post-treatment feature datasets. Subsequently, the difference between each feature pre- and post-treatment was calculated to generate Delta features, resulting in a Delta feature dataset. A total of 851 radiomic features were initially extracted from each VOI in each sequence per patient, including shape features, first-order statistics, higher-order statistics, and wavelet features, summarized in Table 1.

Feature selection and statistical analysis

In this study, Method 1 utilized the Mann-Whitney U test to conduct inter-group difference analysis on MRI radiomic features, identifying significant differences in feature changes between IMRT and IMPT. For these significant features, the degree of change between the two groups was further quantified to assess the impact of IMRT and IMPT on feature variations.

Method 2 involved an additional perspective. Based on dose region distribution, a one-sample t-test was conducted to analyze significant changes within each dose region, incorporating effect size for further filtering, thus identifying features with significant changes in each dose region across both treatment groups. The results

included rankings and effect size visualizations for significant features, providing data support for further clinical application analysis.

Method 1 focused on assessing the presence of significant differences between the distributions of IMRT and IMPT, without considering the magnitude of these changes. Method 2, however, aimed not only to identify significance but also to understand the extent of feature variation. By dividing the mean difference by the standard deviation, effect size was calculated to reflect the actual magnitude of change, offering a complementary, comprehensive analytical perspective.

Method 1 inter-group difference testing for significant features

Data Preparation The Delta feature dataset was read, and data were grouped by treatment type (IMPT and IMRT) and dose regions (high, medium, and low).

Non-parametric test pre- and post-treatment For each feature, pre- and post-treatment changes were assessed for each group (IMPT and IMRT) and each dose region. For each feature, a Wilcoxon signed-rank test was conducted separately in high, medium, and low dose regions for IMPT and IMRT groups. If the p-value for a feature was less than 0.001 across all dose regions for IMPT and IMRT, the feature was considered to exhibit significant change in that dose region for the group and was recorded in the initial significant feature set.

Inter-group non-parametric test A Mann-Whitney U test was conducted on the Delta feature values between IMPT and IMRT groups to identify significant inter-group differences. If the p-value was less than 0.001, it was deemed that the feature exhibited a significant difference in change magnitude between IMPT and IMRT groups. These features were recorded as the final result, representing features with significant pre- and post-treatment changes as well as inter-group differences.

Median percentage change calculation and summary For features selected in the second step, the median change of Delta features was calculated for both IMPT and IMRT groups. If the IMRT group showed a larger median change, the feature was deemed to exhibit a more pronounced change in IMRT; conversely, if IMPT showed a greater change, it was deemed more significant in IMPT. A bar chart displayed the median change magnitudes of selected features between IMPT and IMRT groups to visually indicate the direction and significance of the changes. A pie chart illustrated the proportion of significantly changed features between groups.

Method 2: significant feature selection and effect size ranking

Data Preparation The Delta feature dataset was read, and data were grouped by treatment type (IMPT and IMRT) and dose regions (high, medium, and low).

Significance filtering pre- and post-treatment A one-sample t-test was conducted for each feature in different dose regions and treatment groups, assuming a mean of zero. The p-value and effect size were calculated for each feature, with multiple testing correction using the FDR method. Features with corrected p-values below 0.05 and effect sizes above 0.5 were identified as significant.

Inter-group significance filtering Further inter-group significance testing was conducted on significant features from the first step to assess differences in change magnitude between IMPT and IMRT. For normally distributed data, an independent-sample t-test was used; otherwise, the Mann-Whitney U test was employed. The p-value and effect size were calculated for each feature in different dose regions, and multiple testing correction was applied using the FDR method. Features with corrected p-values below 0.05 and notable effect sizes were identified as significant.

Change magnitude calculation and summary For features identified in the second step, positive effect size indicated that the feature had a more significant change in the IMPT group; a negative effect size indicated greater change in the IMRT group. A bar chart displayed the median change magnitudes of selected features for IMPT and IMRT, visually indicating the direction and significance of the changes between groups.

Significance testing of feature correlation with dose-volume parameters

Although we have confirmed before the experiment that there is no statistically significant difference in the total prescribed dose between the two patient groups, and we have segmented the regions of interest (ROIs) in proportion to the total prescribed dose, an identical or similar dose percentage does not necessarily imply an entirely uniform local dose distribution. Variations in local dose distribution can still induce distinct biological responses in the tissue microenvironment [10]. Therefore, it is necessary to examine the correlation between the final set of significantly effective features and the absolute dose-volume parameters V30, V40, and V50. This correlation analysis will help determine whether the observed inter-group differences in feature variations are genuinely attributable to differences in radiotherapy modalities or are instead influenced by dose distribution heterogeneity.

Visualization of feature variation differences

To intuitively illustrate the extent of brain tissue changes across different dose regions following radiotherapy, we will use box plots and dose distribution-feature variation mapping. These visualizations will effectively depict the magnitude of post-radiotherapy alterations in brain tissue at various dose levels.

Results

Patient's baseline data

The demographic and clinical characteristics comparison are shown in Table 2. Detailed baseline data of the patients can be found in Appendix 1.

Patient dose distribution

The dose distribution trend for the IMPT group was 5713.63 ± 774.32 cGy, while for the IMRT group, it was 5489.86 ± 627.05 cGy. Test results, shown in Table 3, indicate no statistically significant difference. The overall prescription dose distributions for the two groups are illustrated in Fig. 3.

Non-parametric test results: inter-group differences in significant features

The bar chart (Fig. 4) shows that most features identified through Method 1 exhibit more substantial changes in the IMRT group, with a higher percentage change compared to significant changes in the IMPT group. It is noteworthy that here, "percentage change" refers to the median value of a given feature's change within its significantly changed group, standardized as a percentage.

Table 2 Demographic and clinical characteristics comparison

	IMPT	IMRT
	n = 44	*n* = 69
Gender (M/F)	16/28	35/34
Subtentorial involment(Y/N)	31/13	62/7
Deep brain involment(Y/N)	30/14	55/14
Sellar region involment(Y/N)	28/16	42/27

Table 3 Test results of dose distribution difference

	stat	p_val
T test	1.69	0.09
Mann-Whitney U test	1650	0.42

This differs from "effect size," calculated through means and standard deviations in Method 2. Due to the large number of features retained after non-parametric testing in Method 1, a pie chart (Fig. 5) is used to intuitively display the percentage of features with significant changes in each group.Details of the statistical test data of method 1 are shown in appendix 2.

Effect size and multiple testing results: significant feature selection

After multiple testing correction and effect size filtering, 34 features were identified. In some dose regions, certain features were excluded due to stringent correction criteria, but this did not affect the overall data trends or results. The feature selection process is shown in Fig. 6. Details of the statistical test data of method 2 are shown in appendix 3 and appendix 4.

Fig. 3 Total prescription dose distribution bar chart for both patient groups, with green representing the IMPT group and orange representing the IMRT group

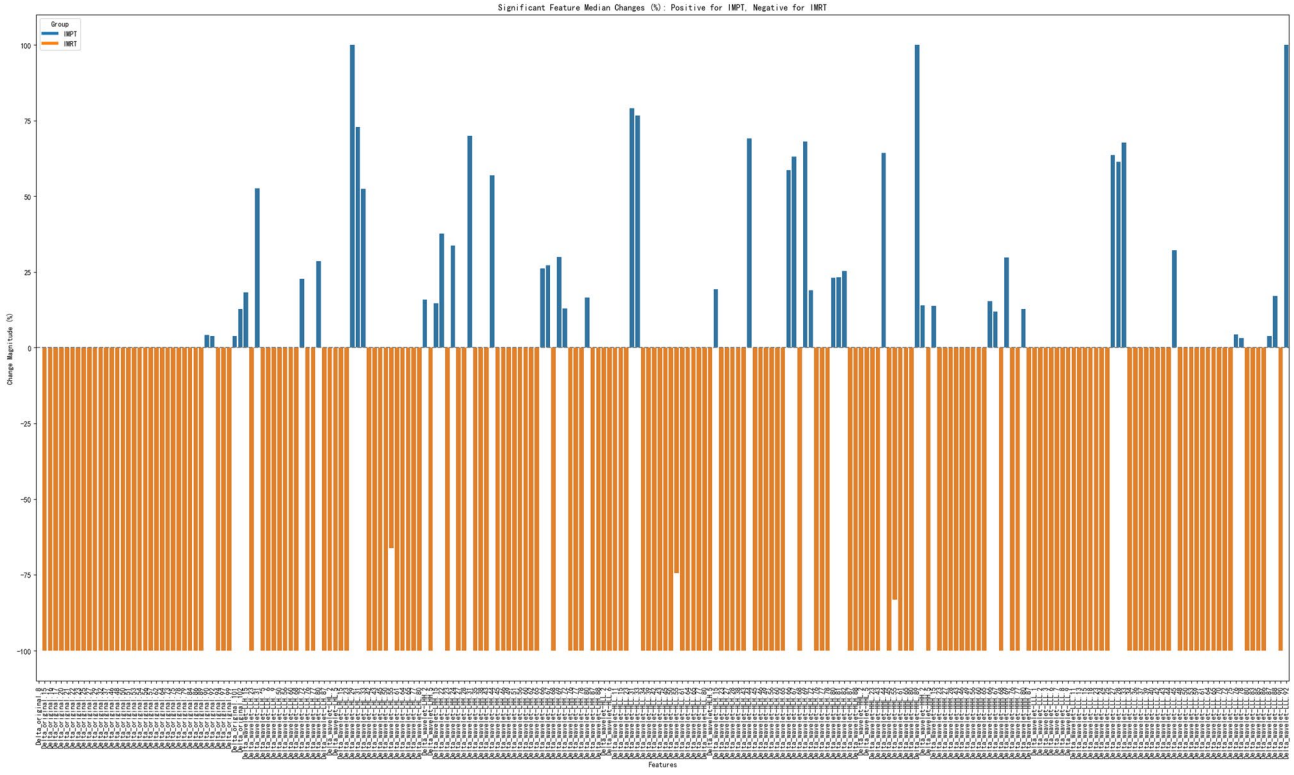

Fig. 4 Bar chart of feature changes in each group as identified by Method 1. The x-axis represents feature names, and the y-axis represents the percentage change in features, standardized by median. Blue bars indicate features with significant changes in the IMPT group, while yellow bars indicate significant changes in the IMRT group

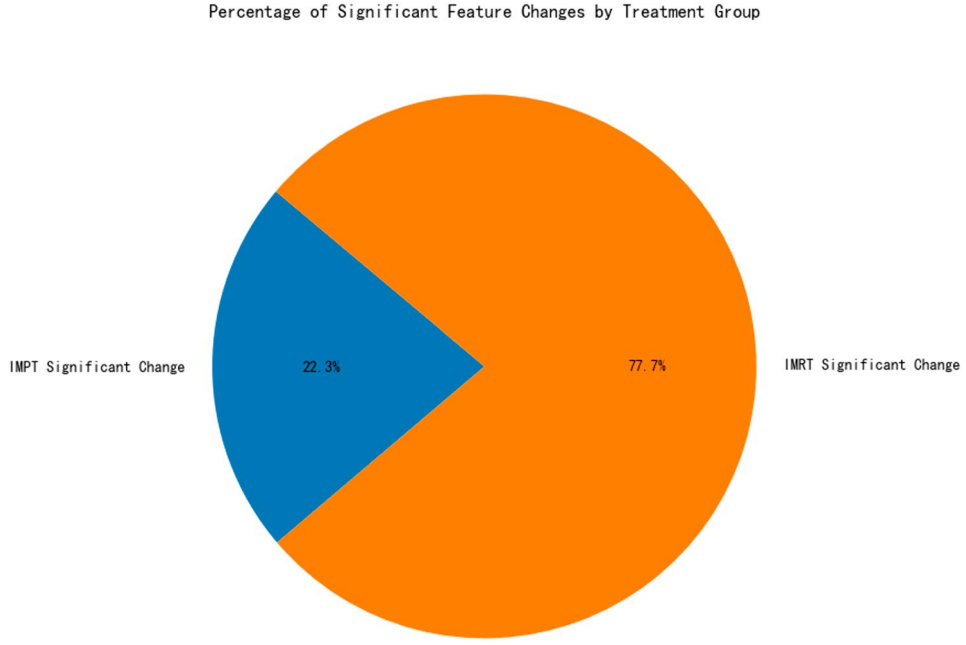

Fig. 5 Pie chart showing the percentage of features with significant changes in each group as identified by Method 1. Blue represents the percentage of features with significant changes in the IMPT group, and yellow represents the percentage in the IMRT group

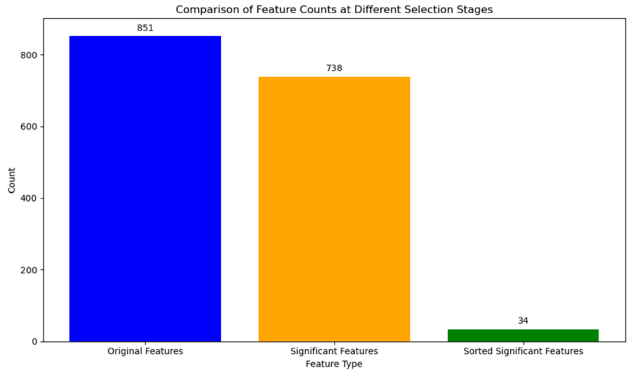

Fig. 6 Initial features are shown in blue. Yellow represents the features with significant changes pre- and post-treatment in all dose regions of both patient groups after the first filtering. Green indicates the 34 features selected in the second filtering phase, showing significant changes between the two groups, which were used for subsequent analysis

Comparison of feature changes between groups based on effect size

Cohen's d method was used to calculate effect size based on the mean difference, quantifying the magnitude of feature changes between the two groups. As shown in Fig. 7, most of the 34 features had negative values with relatively high absolute values, indicating that the majority of features showed more significant changes in the IMRT group.

Correlation analysis of significantly effective features with dose-volume parameters

To further verify whether the observed changes in radiomic features are primarily mediated by different radiotherapy modalities or influenced by dose distribution heterogeneity, a correlation analysis was conducted between the 34 selected radiomic features and the absolute dose-volume parameters. Previous studies have reported that in patients undergoing single or multiple sessions of stereotactic radiotherapy, the risk of radiation-induced necrosis significantly increases when the V30 (volume of normal brain tissue receiving at least 30 Gy) exceeds 10.5 cm^3 [11]. Another study on carbon-ion radiotherapy for brain tumors found that V40 and V50 were associated with the occurrence of ≥ Grade 2 radiation-induced brain injury: Patients with V40 ≥ 7.6 ml had a 38.1% (95% CI: 15.6–60.6%) incidence of ≥ Grade 2 brain injury within 5 years, whereas those with V40 < 7.6 ml had a significantly lower incidence of 10.0% (95% CI: 0–28.6%) ($p = 0.0117$). Patients with V50 ≥ 4.6 ml had a 34.3% (95% CI: 11.5–57.2%) incidence of ≥ Grade 2 brain injury within 5 years, compared to 15.6% (95% CI: 0–35.6%) in those with V50 < 4.6 ml ($p = 0.0192$). Multivariate analysis identified V50 as an independent risk factor for ≥ Grade 2 radiation-induced brain injury following carbon-ion radiotherapy ($p = 0.004$, hazard ratio = 1.229, 95% CI: 1.069–1.412) [12].

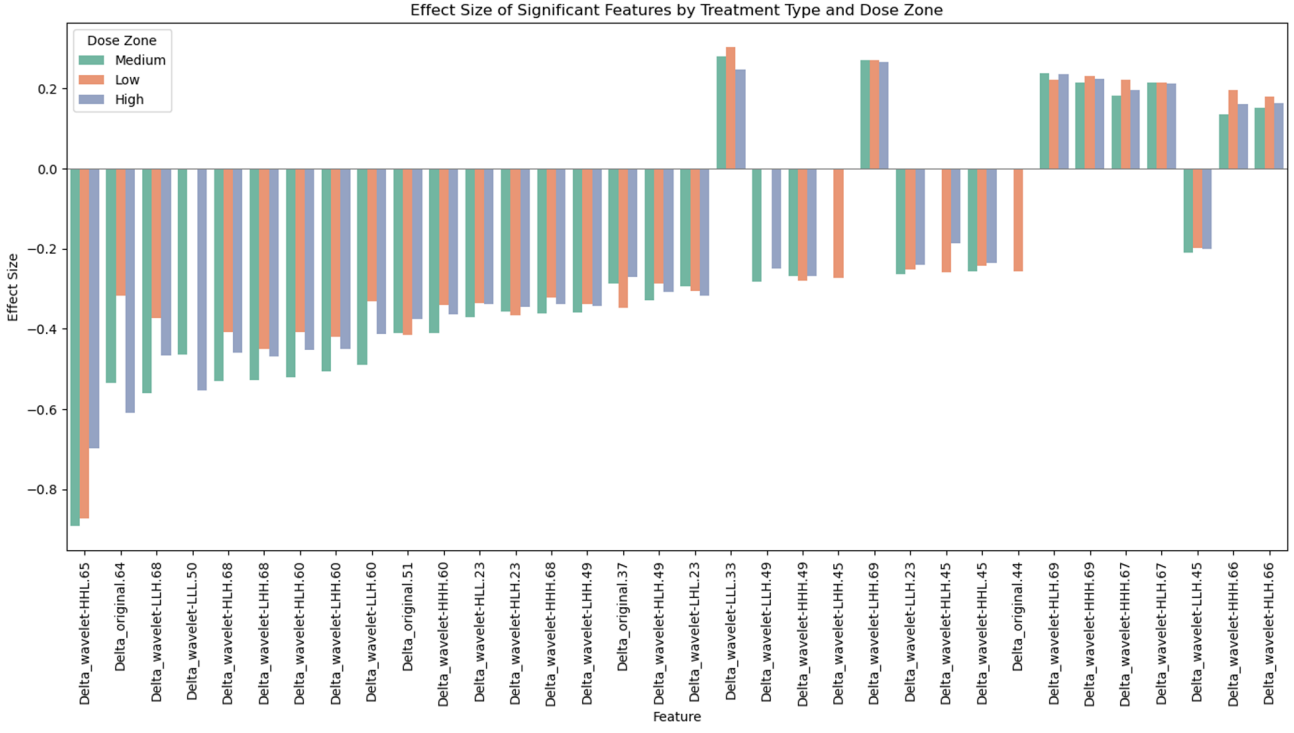

Fig. 7 Cohen's d analysis. Larger absolute effect sizes indicate greater differences in a feature between the two groups. A positive effect size suggests that the feature change is more pronounced in the IMPT group, while a negative effect size indicates a more significant change in the IMRT group

Based on these prior findings and the actual prescribed total dose in the patient cohorts of this study, V30, V40, and V50 were selected for correlation analysis with significantly effective radiomic features. For details on the dose-volume parameters of each patient, please refer to Appendix 5. Results with correlation coefficients (r) > 0.2 and $p < 0.05$ are presented in Tables 4 and 5. 33 out of 34 features showed weak correlations ($r < 0.3$) with dose-volume parameters, suggesting that their variations are more likely mediated by differences in radiotherapy modalities rather than by dose distribution heterogeneity.

When analyzing correlations using absolute volume-absolute dose parameters (cm^3-Gy), the feature Delta_wavelet-HHL.65 exhibited the highest effect size (-0.8) and strong correlations with V30 and V40 in high-dose regions ($r = 0.65$, $p < 0.001$). In medium-dose regions, the correlation coefficients with V30 and V40 were slightly lower ($r = 0.64$ and 0.47, $p < 0.001$), indicating that this feature is significantly influenced by local dose distribution in medium-to-high dose areas. In low-dose regions, its correlation with dose-volume parameters was weaker, suggesting that factors beyond dose distribution may contribute to feature variations.

When using relative volume-absolute dose parameters (%-Gy), the correlation coefficients were generally low, with the highest value being $r = 0.34$. This suggests that absolute volume-based parameters better reflect feature variation trends, whereas relative volume-based parameters may be influenced by inter-patient differences in brain size, leading to larger variability in dose-volume distribution across individuals.

Visualization of feature change differences based on effect size

The top 10 features with the most significant differences in effect size were selected for box plot visualization, as shown in Fig. 8. The median values of features in the IMRT group deviated further from the baseline, suggesting more pronounced changes, consistent with the effect size results. Additionally, box plots for the IMPT group are narrower, indicating smaller and more stable feature changes. Some outliers are observed, likely due to the substantial pre- and post-treatment changes in these selected features, resulting in a marked positive or negative deviation.

Mapping of dose distribution and differences in radiomics feature variation

As shown in Fig. 9, the magnitude of radiomic feature variations for both patient groups is mapped to the corresponding dose regions, visually illustrating the microstructural changes in brain tissue across different dose zones following radiotherapy. The color gradient from dark to light represents the intensity of feature variations from high to low. The IMRT group exhibits significantly greater feature variation intensity than the IMPT group (indicated by darker colors).

The magnitude of variation was derived from the 33 features that were previously confirmed to have low correlation ($r < 0.3$) with dose-volume parameters, ensuring that dose distribution was not the primary influencing factor. After aggregating these features, the results suggest that the observed variations are more likely mediated by distinct microstructural effects induced by different radiotherapy modalities rather than differences in dose distribution. This finding implies that the biological effects of radiotherapy may extend beyond the mere physical dose distribution, advocating for a biologically-driven evaluation framework for radiotherapy techniques rather than one solely based on physical dose metrics.

Discussion

How radiomic features map microstructural changes in brain tissue after radiotherapy

The key radiomic features selected in this study include the Gray-Level Co-Occurrence Matrix (GLCM), Gray-Level Run-Length Matrix (GLRLM), and Gray-Level Size Zone Matrix (GLSZM). GLCM describes the spatial distribution relationships of pixel intensity values. GLRLM measures the continuity of identical gray-level values in an image. GLSZM reflects the homogeneity of pixel regions. These features are considered to indirectly reflect local brain tissue perfusion, tissue heterogeneity,

Table 4 Spearman correlation analysis between feature changes and relative dose-volume parameters

Relative Dose-Volume Parameters(%-Gy)	Feature	Dose	Spearman Correlation	*p*-value
V30	Delta_original.37	Medium	0.21	5.77×10^{-7}
V40	Delta_original.51	High	0.23	4.58×10^{-8}
V30	Delta_original.51	Medium	0.26	1.88×10^{-10}
V40	Delta_wavelet-HHL.45	High	0.23	5.65×10^{-8}
V30	Delta_wavelet-HHL.45	Medium	0.22	9.87×10^{-8}
V40	Delta_wavelet-HHL.65	High	0.34	2.04×10^{-16}
V30	Delta_wavelet-HHL.65	Medium	0.34	6.48×10^{-17}
V30	Delta_wavelet-LLH.60	Medium	0.20	9.79×10^{-7}
V30	Delta_wavelet-LLH.68	Medium	0.22	1.41×10^{-7}

Table 5 Spearman correlation analysis between feature changes and absolute dose-volume parameters

Absolute Dose-Volume Parameters(cm^3-Gy)	Feature	Dose	Spearman Correlation	*p*-value
V40	Delta_original.51	High	0.22	1.43×10^{-7}
V50	Delta_original.51	High	0.22	7.91×10^{-8}
V30	Delta_original.51	Medium	0.26	7.17×10^{-10}
V40	Delta_original.51	Medium	0.26	4.50×10^{10}
V30	Delta_original.64	High	0.25	1.24×10^{-9}
V40	Delta_original.64	High	0.27	1.17×10^{-10}
V50	Delta_original.64	High	0.23	2.38×10^{-8}
V30	Delta_original.64	Medium	0.22	8.03×10^{-8}
V50	Delta_wavelet-HHL.45	High	0.25	1.01×10^{-9}
V30	Delta_wavelet-HHL.45	Medium	0.29	6.41×10^{-13}
V40	Delta_wavelet-HHL.45	Medium	0.25	2.85×10^{-9}
V40	Delta_wavelet-HHL.45	High	0.23	4.81×10^{-8}
V30	Delta_wavelet-HHL.45	High	0.21	7.25×10^{-7}
V30	Delta_wavelet-HHL.65	Medium	0.64	3.81×10^{-65}
V50	Delta_wavelet-HHL.65	High	0.48	6.49×10^{-34}
V30	Delta_wavelet-HHL.65	High	0.65	3.41×10^{-70}
V40	Delta_wavelet-HHL.65	Medium	0.47	5.02×10^{-32}
V40	Delta_wavelet-HHL.65	High	0.65	4.40×10^{-69}
V30	Delta_wavelet-HHL.65	Low	0.24	5.40×10^{-9}
V30	Delta_wavelet-HLH.23	Medium	0.22	1.94×10^{-7}
V40	Delta_wavelet-HLH.60	High	0.24	7.99×10^{-9}
V30	Delta_wavelet-HLH.60	High	0.23	2.68×10^{-8}
V40	Delta_wavelet-HLH.60	Medium	0.20	1.49×10^{-6}
V30	Delta_wavelet-HLH.60	Medium	0.24	6.33×10^{-9}
V30	Delta_wavelet-HLH.68	Medium	0.24	4.07×10^{-9}
V30	Delta_wavelet-HLH.68	High	0.24	8.38×10^{-9}
V40	Delta_wavelet-HLH.68	High	0.25	2.68×10^{-9}
V50	Delta_wavelet-HLH.68	High	0.20	1.38×10^{-6}
V30	Delta_wavelet-LHH.60	High	0.21	1.77×10^{-7}
V40	Delta_wavelet-LHH.60	High	0.23	5.97×10^{-8}
V30	Delta_wavelet-LHH.60	Medium	0.24	1.25×10^{-8}
V30	Delta_wavelet-LHH.68	Medium	0.24	1.34×10^{-8}
V40	Delta_wavelet-LHH.68	High	0.23	2.82×10^{-8}
V30	Delta_wavelet-LHH.68	High	0.23	5.71×10^{-8}
V30	Delta_wavelet-LLH.49	Medium	0.20	1.64×10^{-6}
V30	Delta_wavelet-LLH.60	High	0.24	6.00×10^{-9}
V40	Delta_wavelet-LLH.60	High	0.26	7.45×10^{-10}
V50	Delta_wavelet-LLH.60	High	0.25	3.33×10^{-9}
V30	Delta_wavelet-LLH.60	Medium	0.28	1.42×10^{-11}
V40	Delta_wavelet-LLH.60	Medium	0.24	1.44×10^{-8}
V40	Delta_wavelet-LLH.68	Medium	0.25	8.66×10^{-10}
V30	Delta_wavelet-LLH.68	Medium	0.30	5.20×10^{-14}
V30	Delta_wavelet-LLH.68	High	0.28	2.78×10^{-11}
V40	Delta_wavelet-LLH.68	High	0.29	4.09×10^{-12}
V50	Delta_wavelet-LLH.68	High	0.26	2.50×10^{-10}
V30	Delta_wavelet-LLL.33	Medium	-0.21	2.77×10^{-7}
V30	Delta_wavelet-LLL.50	Medium	0.20	1.51×10^{-6}
V50	Delta_wavelet-LLL.50	High	0.22	1.25×10^{-7}
V30	Delta_wavelet-LLL.50	High	0.23	1.89×10^{-8}
V40	Delta_wavelet-LLL.50	High	0.24	3.68×10^{-9}

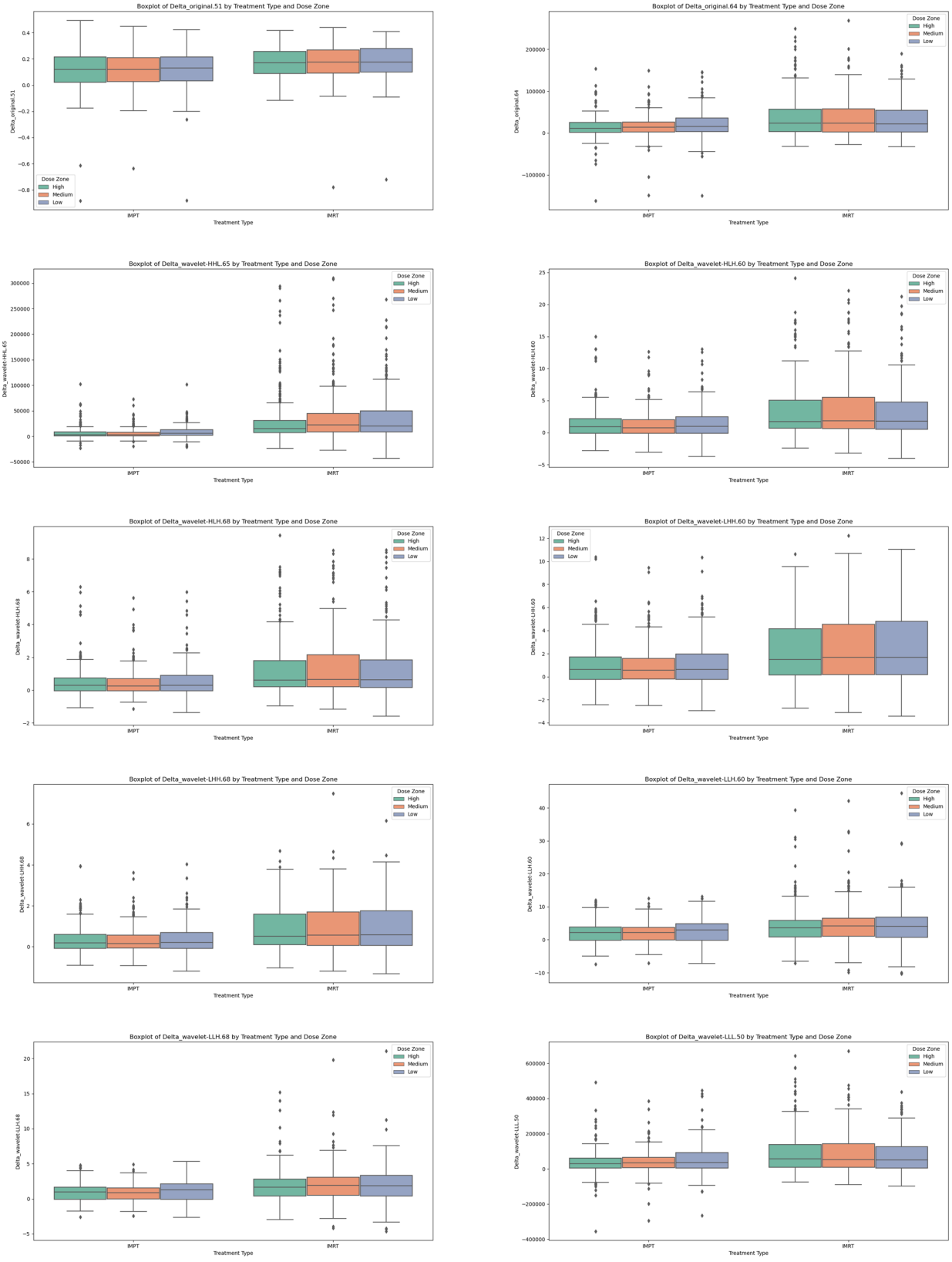

Fig. 8 Box plots for the top 10 features with the highest effect sizes based on Cohen's d method. The IMPT group is on the left, and the IMRT group on the right, with different colors representing different dose regions

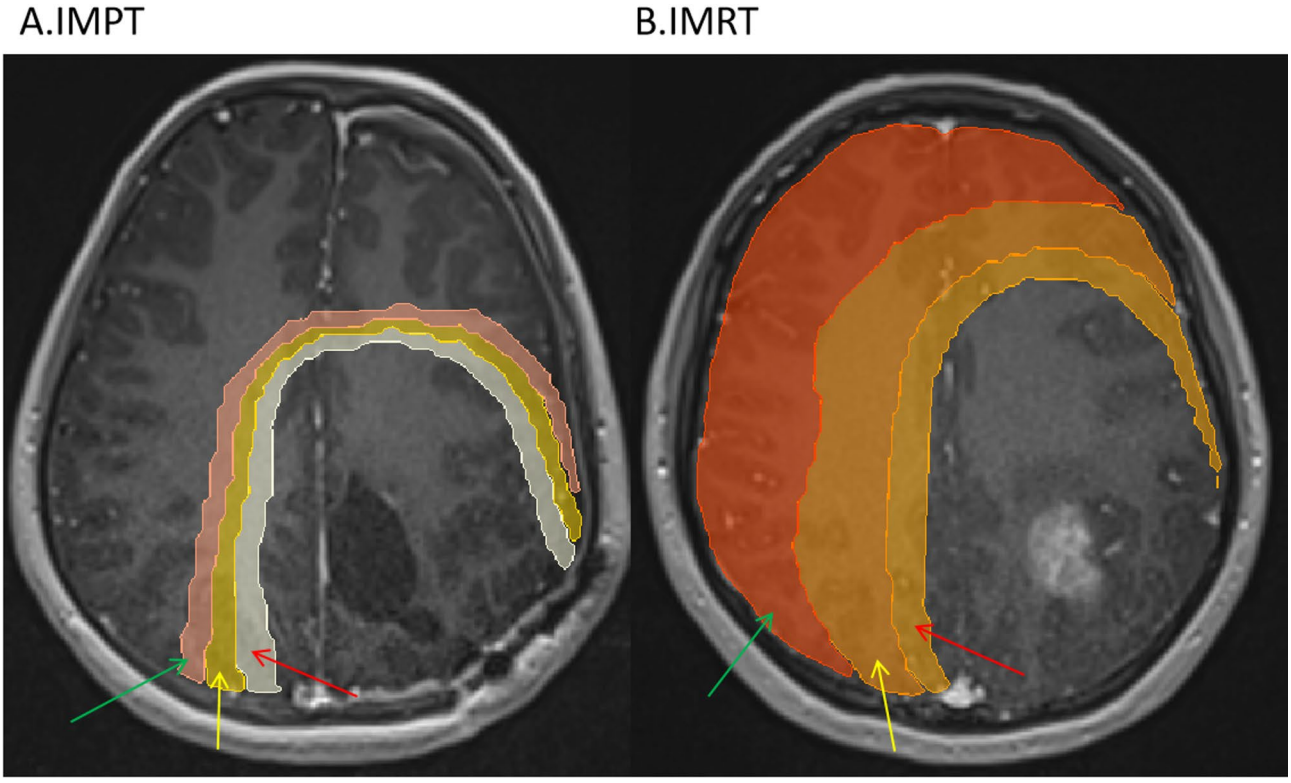

Fig. 9 Mapping of dose distribution and differences in radiomics feature variation

and microstructural changes induced by radiotherapy [13, 14].

A review of recent studies on radiotherapy-induced brain injury reveals that these radiomic features are frequently used for analysis. For example, Chen et al. utilized multi-sequence MRI images and found that radiotherapy-induced white matter damage was primarily associated with GLCM and GLSZM features. They further developed a dose-radiomics model to predict radiation-induced brain injury [15]. Similarly, Zhang et al. demonstrated that GLCM and GLRLM features could effectively differentiate radiation-induced brain injury from tumor recurrence, improving clinical decision-making [16].

These findings indicate that GLCM, GLRLM, and GLSZM align with radiomic features identified in previous studies on radiotherapy-induced brain injury, further validating their clinical significance and interpretability.

Analysis of differences in feature variations in similar dose regions between photon and proton groups

Principles and differences in biological effects during photon and proton interactions with tissue

When photons penetrate tissue, they trigger a series of ionization reactions, generating reactive oxygen species (ROS) and free radicals. These ROS induce oxidative stress, leading to damage in essential intracellular molecular structures [17]. Importantly, ROS and free radicals produced by photon irradiation are not confined to the target region; instead, they widely diffuse through normal tissues along the beam path, causing substantial collateral damage to surrounding healthy tissue [18]. In contrast, protons release energy in a localized manner within a specific region and do not exhibit the same widespread diffusion as photons [19].

Additionally, photon irradiation can activate pro-inflammatory responses by inducing sphingomyelin cleavage, thereby exacerbating tissue damage [20, 21]. Protons, however, induce less activation of the sphingomyelin pathway, resulting in a weaker inflammatory response. As a result, normal tissues exposed to protons experience significantly lower levels of inflammation and oxidative stress compared to those exposed to photons [22].

Mechanisms and differences in radiation-induced tissue damage and repair

DNA damage caused by photon radiation is primarily repaired through a relatively error-prone pathway known as non-homologous end joining (NHEJ). While NHEJ is a rapid repair mechanism, it lacks a template for accurate repair, often leading to incomplete or erroneous DNA repair. This can result in genomic instability, triggering

increased cell death, mutations, and other cellular stress responses, such as apoptosis and necrosis [23, 24].

Conversely, DNA damage induced by proton radiation is repaired through a more precise repair mechanism known as homologous recombination repair (HRR), which has a lower error rate [25]. Therefore, IMRT is more likely to cause higher levels of DNA damage accumulation and more extensive tissue structural alterations in normal tissues compared to IMPT.

Comparison with previous studies

Comparison with previous dose distribution-based brain injury prediction studies

Upadhyay et al. investigated the dose-volume tolerance of brain tissue in a three-fraction stereotactic radiotherapy regimen and identified V20 > 10 cm^3 as an independent predictor of symptomatic necrosis rather than total dose alone [26]. This study emphasized the critical role of localized dose peaks in radiation-induced brain injury, aligning with our finding that Delta_wavelet-HHL.65 exhibited the highest correlation in medium-to-high dose regions (maximum correlation coefficient $r = 0.65$, $p < 0.001$). This suggests that dose-volume constraints can partly explain microstructural damage.

However, we also observed that the remaining 33 radiomic features had weak correlations with dose-volume parameters ($r < 0.3$), indicating that their variations are primarily mediated by radiotherapy modality rather than dose distribution alone. This finding is consistent with the study by Gorbunov et al., who demonstrated that even under the same dose conditions, different radiation particle types induce distinct microvascular damage patterns [27]. Thus, our study further supports the potential of radiomics as a biological dose assessment tool, suggesting that traditional dose-volume histogram (DVH) assessments could be further refined to better capture biological effects.

Comparison with previous radiomics-based brain injury prediction studies

Radiomics has been increasingly applied in predicting radiotherapy-induced toxicity. Salvestrini et al. conducted a retrospective analysis of radiomic feature variations following stereotactic radiotherapy and found that the combination of MRI and PET-CT radiomic features demonstrated a high predictive accuracy for radiation-induced injury (AUC = 0.89) [28]. However, this study primarily focused on a single radiotherapy modality (IMRT) and did not compare the effects of different radiotherapy techniques on the brain's microenvironment. Our study introduces a novel approach by simultaneously comparing radiomic feature variations between IMRT and IMPT. Additionally, we implemented dose distribution-radiomic feature mapping, providing an intuitive visualization of radiomic feature variations within different dose regions.

Furthermore, Lee et al. evaluated the generalizability of radiomic features in CT and MRI imaging across different organs (lung, kidney, and brain). Their study analyzed 2,450 patients and extracted MRI-based radiomic features from multiple anatomical regions. The results showed that radiomic features exhibited greater inter-patient variability in soft tissues, such as the kidney and brain, compared to solid structures like the lung and bone. GLSZM and wavelet-transformed features displayed significant variations across different organs, with AUC values ranging from 0.79 to 0.92 in predicting disease progression [29]. Their findings emphasize the organ-dependent nature of GLSZM and wavelet-transformed features, which aligns with our identification of Delta_wavelet-HHL.65 as a key radiomic feature in post-radiotherapy brain tissue assessment.

Innovative positioning of this study

Filling the gap in existing research

Previous studies have confirmed the differences in macroscopic dose distribution between IMRT and IMPT; however, dosimetric parameters alone cannot capture the dynamic impact of radiotherapy on the tumor or normal tissue microenvironment. This study is the first to utilize longitudinal radiomic feature analysis to reveal that, within target regions receiving similar dose distributions, the IMRT group exhibited significantly greater radiomic feature variations one month post-radiotherapy compared to the IMPT group.

This finding highlights that: similar dose distribution ≠ equivalent biological effects. Even when both techniques achieve a comparable physical dose in the same target region, IMRT may induce more pronounced early microenvironmental alterations, potentially due to a broader low-dose bath or secondary neutron radiation [30]. These alterations may include increased vascular permeability and extracellular matrix remodeling.

Moreover, radiomic features have the potential to serve as biological dose markers, capturing microstructural heterogeneity that conventional dose-volume histograms (DVH) fail to reflect. This provides a new dimension for refining personalized radiotherapy strategies.

Clinical significance of short-term follow-up results

Although this study does not include long-term follow-up data, short-term radiomic feature variations still hold significant clinical value. While short-term follow-up cannot directly predict long-term toxicity, this study utilizes radiomics to detect early differences in the effects of IMRT and IMPT, aligning with the "radiotherapy microenvironmental window" hypothesis proposed by Zhou et al. [31]. This theory suggests that early microstructural

changes may act as initiators of long-term complications. The more pronounced feature variations observed in the IMRT group indicate the need for enhanced early functional imaging surveillance in these patients, which could aid in the early detection and mitigation of potential long-term adverse effects.

Significance of study findings in optimizing radiotherapy strategies

Providing new insights for enhancing traditional dosimetric assessment and promoting the clinical application of IMPT

This study found that IMRT and IMPT induce different MRI feature variations in normal brain tissue, even under similar physical dose conditions, and that most of these features exhibit weak correlations with dose-volume parameters. Therefore, it is reasonable to hypothesize that these short-term feature variations are primarily driven by distinct microenvironmental responses induced by different radiotherapy modalities, rather than heterogeneity in local dose-volume distribution. This finding holds practical significance in complementing and refining the traditional dosimetric evaluation system, advocating for a biological-effect-oriented evaluation standard in radiotherapy. However, it is important to emphasize that this phenomenon is based on short-term observations, and future studies with long-term follow-up are required for further validation.

Additionally, these findings provide new evidence to support the clinical adoption of IMPT, demonstrating that IMPT may not only reduce radiation dose to normal tissues but also minimize microstructural damage load. Furthermore, for cases requiring a balance between target coverage and microenvironmental sensitivity, such as pediatric tumors or genetically susceptible populations, radiomic feature analysis could serve as a valuable tool for treatment selection and risk stratification.

Clinical value of radiomic features in optimizing radiotherapy strategies

This study is the first to conduct a systematic radiomic feature comparison between IMRT and IMPT groups and found that the Delta_wavelet-HHL.65 feature exhibited a large effect size (-0.8) in the IMRT group. Additionally, this feature demonstrated moderate-to-strong correlations with dose-volume parameters in the medium-to-high dose regions, suggesting that its variations may reflect local dose distribution, making it a potential tool for radiotherapy dose optimization and imaging biomarker applications.

Personalized Radiotherapy Optimization: Real-time monitoring of Delta_wavelet-HHL.65 variations could enable dynamic dose adjustments during radiotherapy, optimizing target coverage while minimizing unnecessary exposure to normal brain tissue. In dose-sensitive regions, particularly medium-to-high dose areas, variations in this feature could serve as a key reference for radiotherapy adjustments.

Potential Applications as a Post-Radiotherapy Imaging Biomarker: Delta_wavelet-HHL.65 may serve as an early predictor of radiation-induced injury. Regular MRI-based radiomic analysis could enable the early detection of potential radiation-induced damage, guiding timely clinical interventions, such as adjusting radiotherapy plans or administering neuroprotective agents to mitigate adverse effects.

Study limitations

First, this study is retrospective and may be subject to potential selection bias. Second, the sample size is relatively small, mainly due to the recent introduction of proton therapy in mainland China and its relatively high cost. Third, this study only compared target region feature changes between the two radiotherapy modalities without collecting clinical outcomes to build a model for in-depth exploration. Fourth, the biological processes underlying each selected feature were not fully investigated, which may require further experimental research, such as radiopathological analysis, to deepen understanding of RT-associated brain injuries.

Conclusion

This study, using radiomics analysis, revealed significant differences in the effects of IMRT and IMPT on normal brain tissue, even under similar physical dose conditions. Although the two radiotherapy modalities exhibited comparable dose-volume parameters, the variations in most radiomic features (33 out of 34) showed no significant correlation with dose-volume parameters ($r < 0.3$). This suggests that differences in radiotherapy-induced biological effects may extend beyond physical dose distribution, highlighting the potential for refining the traditional dosimetric evaluation system and advancing biologically-driven radiotherapy assessment standards.

Additionally, the feature Delta_wavelet-HHL.65 exhibited the most significant changes in the IMRT group and demonstrated strong correlations with dose-volume parameters, making it a promising predictor for radiotherapy dose optimization in clinical practice. Future research should further explore radiomics-dosimetry combined modeling and the application of machine learning in radiotherapy optimization, facilitating the implementation of personalized radiotherapy strategies.

Abbreviations

MRI	Magnetic resonance imaging
IMRT	Intensity-modulated radiation therapy
IMPT	Intensity-modulated proton therapy
T2FLAIR	T2 fluid-attenuated inversion recovery sequence
ADC	Apparent diffusion coefficient
VOI	Volumes of interest

RT	Radiotherapy
AUC	Areas under the curve
RTLI	Radiation-induced temporal lobe injury
ROS	Reactive oxygen species
DNA	Deoxyribonucleic acid
HRR	Homologous recombination repair
NHEJ	Non-homologous end joining
RBE	Relative biological effectiveness
LET	Linear energy transfer

Supplementary Information

The online version contains supplementary material available at https://doi.org/10.1186/s12880-025-01724-y.

Supplementary Material 1

Supplementary Material 2

Supplementary Material 3

Supplementary Material 4

Supplementary Material 5

Acknowledgements
Not applicable.

Author contributions
J.X. was responsible for data collection, processing, and the primary drafting of the manuscript. L.Z. conducted the literature review. T.L. and Q.L. prepared the figures and tables. Z.J. provided guidance and revisions.

Funding
This work was supported by Gansu Province Nature Science Foundation (24JRRA1152),the National Natural Science Foundation of China (82172072) and the Foundation of Shandong Provincial Key Research and Development(2024CXPT084).

Data availability
The datasets generated and analyzed during the current study are not publicly available due to patient privacy and confidentiality concerns. However, the data can be made available from the corresponding author upon reasonable request and approval by the institutional ethics committee.

Declarations

Ethics approval and consent to participate
This study was consistent with the principles expressed in the Declaration of Helsinki and approved by the Ethics Committee of Shandong Cancer Hospital and Institute (Ethics number: SDTHEC202411012). The informed consent was waived for this retrospective study.

Consent for publication
Not applicable.

Competing interests
The authors declare no competing interests.

Author details
[1]Department of Radiation Physics Technology, Shandong Cancer Hospital and Institute, Shandong First Medical University, Shandong Academy of Medical Sciences, Jinan 250117, P. R. China
[2]Shandong Provincial Key Medical and Health Laboratory of Pediatric Cancer Precision Radiotherapy (Shandong Cancer Hospital), Jinan 250117, P. R. China
[3]Liaocheng People's Hospital of Shandong Province, Liaocheng 252000, P. R. China
[4]Sun Yat-sen University Cancer Center Gansu Hospital, Lanzhou 730050, P. R. China

Received: 28 November 2024 / Accepted: 12 May 2025
Published online: 21 May 2025

References

1. Chang C-L, Lin K-C, Chen W-M, Shia B-C. Szu-Yuan Wu.Comparing the oncologic outcomes of proton therapy and intensity-modulated radiation therapy for head and neck squamous cell carcinoma. Radiother Oncol. 2024;190:109971.
2. Cortiula F, Hendriks LEL, Wijsman R, Houben R, Steens M, Debakker S, Canters R, Trovò M, Sijtsema NM, Niezink AGH, Unipan M, Urban S, Michelotti A, Dursun S, Bootsma G, Hattu D, Nuyttens JJ, Moretti E, Taasti VT, De Ruysscher D. Proton and photon radiotherapy in stage III NSCLC: effects on hematological toxicity and adjuvant immune therapy. Radiother Oncol. 2024;190:110019.
3. Johnson PB, Mamalui M, Brodin P, Janssens G. Secondary cancer risk in six anatomical sites when using PAT, IMPT, and VMAT/IMRT radiotherapy. Radiother Oncol. 2024;199:110421.
4. Grosshans D, Thomas R, Zhang D, Cronkite C, Thomas R, Singh S, Bronk L, Morales R, Duman J. Subcellular functions of tau mediates repair response and synaptic homeostasis in injury. Res Sq [Preprint]. 2024 Feb 29:rs.3.rs-3897741.
5. Shamsesfandabadi P, Patel A, Liang Y, Shepard MJ, Wegner RE. Radiation-Induced cognitive decline: challenges and solutions. Cancer Manag Res. 2024;16:1043–52.
6. Zhang B, Lian Z, Zhong L, Zhang X, Dong Y, Chen Q, Zhang L, Mo X, Huang W, Yang W, Zhang S. Machine-learning based MRI radiomics models for early detection of radiation-induced brain injury in nasopharyngeal carcinoma. BMC Cancer. 2020;20(1):502.
7. Bao D, Zhao Y, Li L, Lin M, Zhu Z, Yuan M, Zhong H, Xu H, Zhao X, Luo D. A MRI-based radiomics model predicting radiation-induced Temporal lobe injury in nasopharyngeal carcinoma. Eur Radiol. 2022;32(10):6910–21.
8. Hou J, Li H, Zeng B, Pang P, Ai Z, Li F, Lu Q, Yu X. MRI-based radiomics nomogram for predicting Temporal lobe injury after radiotherapy in nasopharyngeal carcinoma. Eur Radiol. 2022;32(2):1106–14.
9. Haga A, Takahashi W, Aoki S, Nawa K, Yamashita H, Abe O, Nakagawa K. Standardization of imaging features for radiomics analysis. J Med Invest. 2019;66(12):35–7.
10. Potiron S, Iturri L, Juchaux M, Espenon J, Gilbert C, McGarrigle J, Ortiz Catalan R, Fernandez-Rodriguez A, Sebrié C, Jourdain L, De Marzi L, Créhange G, Prezado Y. The significance of dose heterogeneity on the anti-tumor response of Minibeam radiation therapy. Radiother Oncol. 2024;201:110577.
11. Milano MT, Grimm J, Niemierko A, Soltys SG, Moiseenko V, Redmond KJ, Yorke E, Sahgal A, Xue J, Mahadevan A, Muacevic A, Marks LB, Kleinberg LR. Single- and multifraction stereotactic radiosurgery dose/volume tolerances of the brain. Int J Radiat Oncol Biol Phys. 2021;110(1):68–86. https://doi.org/10.1016/j.ijrobp.2020.08.013. Epub 2020 Sep 11.
12. Koto M, Hasegawa A, Takagi R, Fujikawa A, Morikawa T, Kishimoto R, Jingu K, Tsujii H, Kamada T. Risk factors for brain injury after carbon ion radiotherapy for skull base tumors. Radiother Oncol. 2014;111(1):25–9.
13. Yang Y, Yan LF, Zhang X, Nan HY, Hu YC, Han Y, Zhang J, Liu ZC, Sun YZ, Tian Q, Yu Y, Sun Q, Wang SY, Zhang X, Wang W, Cui GB. Optimizing texture retrieving model for multimodal MR Image-Based support vector machine for classifying glioma. J Magn Reson Imaging. 2019;49(5):1263–74.
14. Sun T, Yu HY, Zhan CH, Guo HL, Luo MY. Non-contrast CT radiomics-clinical machine learning model for futile recanalization after endovascular treatment in anterior circulation acute ischemic stroke. BMC Med Imaging. 2024;24(1):178.
15. Chen M, Wang L, Gong G, Yin Y, Wang P. Quantitative study of the changes in brain white matter before and after radiotherapy by applying multi-sequence MR radiomics. BMC Med Imaging. 2022;22(1):86.
16. Zhang J, Wu Y, Wang Y, Zhang X, Lei Y, Zhu G, Mao C, Zhang L, Ma L. Diffusion-weighted imaging and arterial spin labeling radiomics features May improve differentiation between radiation-induced brain injury and glioma recurrence. Eur Radiol. 2023;33(5):3332–42.
17. Huang H, Zhang S, Li Y, Liu Z, Mi L, Cai Y, Wang X, Chen L, Ran H, Xiao D, Li F, Wu J, Li T, Han Q, Chen L, Pan X, Li H, Li T, He K, Li A, Zhang X, Zhou T, Xia Q, Man J. Suppression of mitochondrial ROS by prohibitin drives glioblastoma progression and therapeutic resistance. Nat Commun. 2021;12(1):3720.
18. Tattenberg S, Marants R, Niepel K, Bortfeld T, Sudhyadhom A, Landry G, Parodi K, Verburg J. Validation of prompt gamma-ray spectroscopy for proton

range verification in tissue-mimicking and Porcine samples. Phys Med Biol. 2022;67(20). https://doi.org/10.1088/1361-6560/ac950f.
19. Cui Y, Pan Y, Li Z, Wu Q, Zou J, Han D, Yin Y, Ma C. Dosimetric analysis and biological evaluation between proton radiotherapy and photon radiotherapy for the long target of total esophageal squamous cell carcinoma. Front Oncol. 2022;12:954187.
20. Loizeau N, Fabiano S, Papp D, Stützer K, Jakobi A, Bandurska-Luque A, Troost EGC, Richter C, Unkelbach J. Optimal allocation of proton therapy slots in combined proton-Photon radiation therapy. Int J Radiat Oncol Biol Phys. 2021;111(1):196–207.
21. Lin MH, Yang M, Dougherty J, Tasson A, Zhang Y, Mohamad O, Dan T, Yan Y, Gu X, Timmerman R, Laack N, Beltran C. Radiation Therapy for Pediatric Brain Tumors using Robotic Radiation Delivery System and Intensity Modulated Proton Therapy. Pract Radiat Oncol. 2020 May-Jun;10(3):e173–82. https://doi.org/10.1016/j.prro.2019.09.008. Epub 2019 Sep 19. PMID: 31542454.
22. Fabiano S, Bangert M, Guckenberger M, Unkelbach J. Accounting for range uncertainties in the optimization of combined Proton-Photon treatments via stochastic optimization. Int J Radiat Oncol Biol Phys. 2020;108(3):792–801.
23. Eulitz J, Lutz B, Wohlfahrt P, Dutz A, Enghardt W, Karpowitz C, Krause M, Troost EGC, Lühr A. A Monte Carlo based radiation response modelling framework to assess variability of clinical RBE in proton therapy. Phys Med Biol. 2019;64(22):225020.
24. Paganetti H. Mechanisms and review of clinical evidence of variations in relative biological effectiveness in proton therapy. Int J Radiat Oncol Biol Phys. 2022;112(1):222–36.
25. Goudarzi HM, Lim G, Grosshans D, Mohan R, Cao W. Incorporating variable RBE in IMPT optimization for ependymoma. J Appl Clin Med Phys. 2024;25(1):e14207.
26. Upadhyay R, Ayan AS, Jain S, Klamer BG, Perlow HK, Zoller W, Blakaj DM, Beyer S, Grecula J, Arnett A, Thomas E, Chakravarti A, Raval RR, Palmer JD. Dose-Volume tolerance of the brain and predictors of radiation necrosis after 3-Fraction radiosurgery for brain metastases: A large Single-Institutional analysis. Int J Radiat Oncol Biol Phys. 2024;118(1):275–84.
27. Gorbunov NV, Kiang JG. Brain damage and patterns of neurovascular disorder after ionizing irradiation. Complications in radiotherapy and radiation combined injury. Radiat Res. 2021;196(1):1–16.
28. Salvestrini V, Greco C, Guerini AE, Longo S, Nardone V, Boldrini L, Desideri I, De Felice F. The role of feature-based radiomics for predicting response and radiation injury after stereotactic radiation therapy for brain metastases: A critical review by the young group of the Italian association of radiotherapy and clinical oncology (yAIRO). Transl Oncol. 2022;15(1):101275.
29. Vozenin MC, Hendry JH, Limoli CL. Biological benefits of Ultra-high dose rate FLASH radiotherapy: sleeping beauty awoken. Clin Oncol (R Coll Radiol). 2019;31(7):407–15.
30. Chua KLM, Chu PL, Tng DJH, Soo KC, Chua MLK. Repurposing proton beam therapy through novel insights into tumour radioresistance. Clin Oncol (R Coll Radiol). 2021;33(11):e469–81.
31. Demaria S, Guha C, Schoenfeld J, Morris Z, Monjazeb A, Sikora A, Crittenden M, Shiao S, Khleif S, Gupta S, Formenti SC, Vikram B, Coleman CN, Ahmed MM. Radiation dose and fraction in immunotherapy: one-size regimen does not fit all settings, so how does one choose? J Immunother Cancer. 2021;9(4):e002038.

Publisher's note